2019

In Vitro Bioaccessibility of Low-Crystallinity Phytosterol Nanoparticles Generated Using Nanoporous Starch Bioaerogels

Ali Ubeyitogullari
University of Nebraska - Lincoln, aubeyitogullari2@unl.edu

Regis Moreau
University of Nebraska–Lincoln, rmoreau2@unl.edu

Devin J. Rose
University of Nebraska-Lincoln, drose3@unl.edu

Ozan Ciftci
University of Nebraska-Lincoln, ciftci@unl.edu

In Vitro Bioaccessibility of Low-Crystallinity Phytosterol Nanoparticles Generated Using Nanoporous Starch Bioaerogels

Ali Ubeyitogullari,[1] Régis Moreau,[2]
Devin J. Rose,[1] and Ozan N. Ciftci[1]

1 Department of Food Science and Technology, University of Nebraska-Lincoln, Lincoln, NE, 68588-6205

2 Department of Nutrition and Health Sciences, University of Nebraska-Lincoln, Lincoln, NE, 68583-0806

Corresponding author — Ozan N. Ciftci, *email* ciftci@unl.edu

Abstract

Phytosterols are natural health-promoting bioactive compounds; however, phytosterols have very limited bioavailability due to their crystalline lipophilic structure. With the aim of improving bioaccessibility, low-crystallinity phytosterol nanoparticles were generated by supercritical carbon dioxide (SC-CO_2) impregnation of phytosterols into nanoporous starch aerogels (NSAs). The *in vitro* bioaccessibility of the phytosterol nanoparticles (35%) was significantly higher than that of the crude phytosterols (3%) after sequential oral, gastric, and intestinal digestion. The percentages of starch hydrolysis were not different among the various NSA preparations and reached to 64% after sequential digestion. The zeta potential of the phytosterol nanoparticles was higher compared to that of crude phytosterols in the micellar phase; indicating higher stability.

Published in *Journal of Food Science* 84:7 (2019), pp 1812–1819.
doi: 10.1111/1750-3841.14673

Submitted 6 August 2018; accepted 7 May 2019.

The findings of this study support the use of NSA to produce nanoparticles of reduced crystallinity to improve the bioaccessibility of the lipophilic bioactive compounds. Keywords: aerogel, bioaccessibility, nanoparticles, phytosterol, supercritical Practical Applications: This novel process can decrease the size and crystallinity of phytosterols and thus improve phytosterols' bioavailability. It is a blueprint to apply to other water insoluble food bioactives. This novel approach may (i) improve the health benefits of water-insoluble bioactives; (ii) enable food manufacturers to add water-insoluble bioactives into low- and high-fat foods to produce health-promoting foods; and (iii) enhance the cost-benefit ratio of water insoluble bioactives.

Introduction

Phytosterols have received much attention in recent years due to their health benefits such as reduction in serum LDL-cholesterol level (Amir Shaghaghi, Harding, and Jones, 2014; Trautwein et al., 2003), antiatherogenic (Moghadasian, Tan, Le, & Shahidi, 2016) and anticancer effects (Woyengo, Ramprasath, & Jones, 2009), and more recently anti-inflammatory properties (Aldini et al., 2014; Feng et al., 2017; Othman & Moghadasian, 2011). The cholesterol lowering effect is the most commonly studied and well-known health-promoting effect of phytosterols. Phytosterols are homologs of cholesterol but the additional side chain at the C-24 position makes phytosterols more hydrophobic than cholesterol (Moreno-Calvo et al., 2014). According to a recent meta-analysis, daily intake of 0.6 to 3.3 g of phytosterols could reduce LDL-cholesterol by 6 to 12% (Ras, Geleijnse, & Trautwein, 2014).

However, phytosterols are high melting point crystalline lipophilic bioactive compounds with low water solubility, and, in turn, poor bioaccessibility. Bioaccessibility is an important component of nutrient bioavailability. Limited bioaccessibility of the phytosterols in the aqueous phase of the intestinal content is responsible for the poor bioavailability of the phytosterols, leading to only 1.5 to 5% absorption in humans (Nguyen, 1999). Considerable efforts have been recently dedicated to improving the solubility and/or bioavailability of phytosterols. So far, chemoenzymatic modifications (He et al., 2016), emulsion formulations (Fisher, Wachtel, Aserin, & Garti, 2013; Leong et al., 2011; Moschakis, Dergiade, Lazaridou, Biliaderis, & Katsanidis,

2017; Ribeiro et al., 2016; Rozner, Aserin, Wachtel, & Garti, 2007; Zychowski et al., 2016), formation of colloidal phytosterols by precipitation from organic solvents (Rossi, Seijen ten Hoorn, Melnikov, & Velikov, 2010), synthesis of cyclodextrin inclusion complexes (Meng, Pan, & Liu, 2012), cocrystallization of phytosterols and triacylglycerols (Acevedo & Franchetti, 2016), and microencapsulation by spray drying (Di Battista, Constenla, Ramírez-Rigo, & Piña, 2015) have been used for decreasing the particle size and improving the solubility of phytosterols. However, long complicated chemical modifications, the use of toxic organic solvents and nonfood grade surfactants remain major obstacles with these methods.

In recent years, different alternative processes based on supercritical fluid technology have been proposed to form phytosterol particles and overcome these drawbacks; they include rapid expansion of supercritical solution into air (RESS) (Türk & Lietzow, 2008; Türk, Helfgen, Hils, Lietzow, & Schaber, 2002; Türk, Upper, & Hils, 2006), coprecipitation during the rapid expansion of supercritical solutions (CORESS) (Türk et al., 2006), rapid expansion of supercritical solution into aqueous solution (RESSAS) (Türk & Lietzow, 2004), and depressurization of an expanded liquid organic solution (DELOS) (Moreno-Calvo et al., 2014). However, agglomeration of the particles due to collisions, and using organic solvents and surfactants remain important limitations of these techniques.

Very recently, our group introduced a novel method that uses nanoporous starch aerogels (NSAs) to generate low-crystallinity phytosterol nanoparticles using SC-CO_2 (Ubeyitogullari & Ciftci, 2016b, 2017; Ubeyitogullari, Moreau, Rose, Zhang, & Ciftci, 2018). This method eliminates the use of toxic organic solvents and surfactants, and utilizes CO_2 as a solvent that is inexpensive, abundant, nontoxic, environmentally friendly, and has mild critical temperature (31 °C) and pressure (7.4 MPa). In this approach, we have produced NSAs with surface area of 60 m^2/g, density of 0.12 g/cm^3, and pore size of 20 nm (Ubeyitogullari & Ciftci, 2016a). Low-crystallinity phytosterol nanoparticles were formed by recrystallization of phytosterols from a phytosterol-SC-CO_2 solvato complex in the nanopores of the NSAs with a drastic decrease in the solubility of phytosterols in the SC-CO_2. At the optimized particle formation conditions, the phytosterol impregnation capacity was 99 mg/g NSA and the impregnated phytosterols were

nanosized (59 to 87 nm) with reduced crystallinity. Thus, impregnated phytosterols had superior water dissolution rate compared to crude phytosterols (Ubeyitogullari & Ciftci, 2016b, 2017).

Once low-crystallinity phytosterol nanoparticles were generated, the next step was to evaluate their bioaccessibility. The bioaccessibility of phytosterols was improved by impregnating them into wheat and corn starch aerogels in our previous study (Ubeyitogullari et al., 2018). We hypothesized that low-crystallinity phytosterol nanoparticles impregnated in NSA would have superior bioaccessibility compared to crude phytosterols. However, there is a critical need for the evaluation of the aerogels' digestibility in detail as the release of the bioactives after each step of the gastrointestinal digestion affects the stability of bioactives and consequently might impair their bioaccessibility. Thus, the goal of the study was to further evaluate the effect of each digestion step on the NSAs and low-crystallinity phytosterol nanoparticles. Specific objectives were to: (i) form NSAs from wheat starch using $SCCO_2$ drying, (ii) use NSA to form low-crystallinity phytosterol nanoparticles via SC-CO_2, and (iii) determine the bioaccessibility of the low-crystallinity phytosterol nanoparticles after each digestion step and study the effect of phytosterol particle distribution on the bioaccessibility.

Materials and Methods

Materials

Wheat starch was kindly provided by Manildra Milling Corp. (IA, USA). Crude phytosterols (52.1 ± 0.6% β-sitosterol, 23.5 ± 0.3% stigmasterol, and 24.4 ± 0.4% campesterol) were obtained from MP Biomedicals (OH, USA). Liquid CO_2 (purity > 99.99%) was purchased from Matheson Tri-Gas, Inc. (NE, USA). Pyridine was obtained from EMD Chemicals, Inc. (NJ, USA). Sylon BFT [N,O-bis(trimethylsilyl)trifluoroacetamide (BSTFA):trimethylchlorosilane (TMCS), 99:1] was purchased from Supelco Inc. (PA, USA) and 5α-cholestane (>98%) was obtained from Acros Organics (NJ, USA). Ethanol (100%) was obtained from Decon Laboratories, Inc. (PA, USA). α-Amylase (from *Bacillus subtilis*, 160,000 BAU/g, Cat. No. 100447) was obtained from MP Biomedicals

(OH, USA). Pepsin (porcine gastric mucosa, 3,616 U/mg protein, Cat. No. P6887), pancreatin (from porcine pancreas, neutral protease: 208 USP units/mg solid; α-amylase: 223 units/mg solid; lipase: 38.5 USP units/mg solid, Cat. No. 7545), lipase (from porcine pancreas, 419 U/mg protein, Cat. No. L3126) and bile extract (from porcine, Cat. No. B8631) were all purchased from Sigma-Aldrich (MO, USA). Lipase A "Amano" 12 lipase A12 (from fungus *Aspergillus niger*, 132,000 U/g) was kindly provided by Amano Enzyme Inc. (IL, USA). All other chemicals were of analytical grade.

NSA formation

NSA monoliths were produced from wheat starch at the previously optimized NSA formation conditions (Ubeyitogullari & Ciftci, 2016a). Briefly, first, wheat starch was gelatinized in a high-pressure reactor (4520 Bench Top Reactor, Parr Instrument Comp., IL, USA) at 120 °C with a mixing rate of 600 rpm for 20 min to obtain a hydrogel. The hydrogels were kept at 4 °C for 48 hr for retrogradation. Then, the hydrogel was converted to an alcogel by replacing water in the hydrogel with ethanol by a five-step solvent exchange step. Finally, the alcogels were dried by SC-CO_2 at 40 °C, 10 MPa for 4 hr with a CO_2 flow rate of 0.5 L/min (measured at ambient conditions) to obtain the NSAs. The properties of the NSAs were determined according to Ubeyitogullari and Ciftci (2016a), and presented in **Table 1**.

SC-CO2 impregnation of phytosterols into NSAs

Impregnation of phytosterols into NSAs was carried out in a custom laboratory scale SC-CO_2 impregnation system. Details of the system were reported elsewhere (Ubeyitogullari & Ciftci, 2017). Two different SC-CO_2 impregnation methods were selected based on our previous study (Ubeyitogullari & Ciftci, 2017). Briefly, phytosterols (0.5

Table 1. The characteristics of the produced NSAs.

BET surface area (m^2/g)	61.1 ± 2.0
BJH pore size (nm)	18.8 ± 1.1
Pore volume (cm^3/g)	0.27 ± 0.01
Density (g/cm^3)	0.11 ± 0.01
Porosity (%)	92.6 ± 0.2

g) and NSAs (1 g) were wrapped in separate filter papers (Whatman #41, NJ, USA) and placed into the bottom and top compartments of the vessel, respectively. In the first method, the impregnation was carried out at 45 MPa, 90 °C for 3 hr with a semidynamic mode where the shut off valve was opened for 1 min (CO_2 flow of 1 L/min at ambient conditions) every 10 min. Afterwards, the system was cooled to 25 °C at a cooling rate of 10.3 °C/min. Phytosterol-impregnated NSAs were obtained after depressurization of the system at a CO_2 flow rate of 1 L/min (measured at ambient conditions). In the second method, three successive fast cooling cycles within the same run were employed to increase the phytosterol loading capacity (Ubeyitogullari & Ciftci, 2017).Hereafter, phytosterols impregnated into the NSA using the first method and the second method are called as PS-NSA-F and PS-NSA-3F, respectively. Phytosterol impregnation capacity was determined by GC according to the method of Ubeyitogullari and Ciftci (2017) as described in the Phytosterol analysis section and reported as mg phytosterol/g NSA.

Morphology

The morphology of the impregnated phytosterols was analyzed by a field emission scanning electron microscope (S4700 FE-SEM, Hitachi, Tokyo, Japan) under low vacuum mode. The specimens (1-mm thick cross-sections) were directly mounted on aluminum stubs with double-side conductive carbon tape and then coated with chromium using a sputter coater (Desk V HP TSC, Denton Vacuum LLC, NJ, USA) prior to analysis. The coated samples were scanned at an accelerating voltage of 5 kV.

The average particle size of the phytosterols impregnated in the NSAs was determined from the SEM images. The average particle size was estimated from randomly selected 50 particles using ImageJ v. 1.50i software (public domain, Natl. Inst. of Health, USA) (Ubeyitogullari & Ciftci, 2017).

In vitro digestion

Simulated gastrointestinal digestions of PS-NSA-F, PS-NSA-3F, and controls were performed based on the method of Minekus et al.

(2014). Gastrointestinal digestion model consisted of oral, gastric, and intestinal phases. The effect of each of the oral, gastric and intestinal phases on the phytosterol impregnated NSAs were studied separately. A sequential oral, gastric and intestinal digestion was also carried out. Fresh samples were used for each digestion experiment. Simulated digestion of physical mixture of crude phytosterols and empty NSAs (PS-NSA physical mixture), empty NSA, and a blank (digestion medium with the enzymes) were performed as controls.

Oral phase.

Oral phase digestion method was adapted from Minekus et al. (2014) and Mennah-Govela and Bornhorst (2016) with slight modifications. Simulated salivary fluid (SSF) was prepared according to Minekus et al. (2014). SSF electrolyte stock solution composed of various salts (potassium chloride, monopotassium phosphate, sodium bicarbonate, sodium chloride, magnesium chloride hexahydrate, and ammonium carbonate) shown in the **Table 2**. The pH of the solution was adjusted to 7.0 with 1 M HCl. SSF electrolyte stock solution (7 mL) and the sample (0.25 g) were added into an Erlenmeyer flask. One mL of α-amylase solution (750 U/mL) was added to obtain a final mixture of 75 U/mL. Then, 50 µL of 0.3 M $CaCl_2$ and 1.95 mL of deionized water were added and mixed. Finally, pH of the mixture was adjusted to 7 and the mixture was agitated in a shaking water bath (C76 Water Bath Shaker, New Brunswick Scientific, NJ, USA) for 30 seconds at 37 °C at a mixing rate of 150 rpm.

Table 2. Composition of simulated salivary fluid (SSF), simulated gastric fluid (SGF) and simulated intestinal fluid (SIF).

			SSF (pH 7)		*SGF (pH 3)*		*SIF (pH 7)*	
Constituent	*Stock conc.*		*Volume of stock*[a]	*Conc. in SSF*	*Volume of stock*[a]	*Conc. in SGF*	*Volume of stock*[a]	*Conc. in SIF*
	g/L	mol/L	mL	mmol/L	mL	mmol/L	mL	mmol/L
KCl	37.3	0.5	7.55	15.1	3.45	6.9	3.4	6.8
KH_2PO_4	68	0.5	1.85	3.7	0.45	0.9	0.4	0.8
$NaHCO_3$	84	1	3.4	13.6	6.25	25	21.25	85
NaCl	117	2	—	—	5.9	47.2	4.8	38.4
$MgCl_2(H_2O)_6$	30.5	0.15	0.25	0.15	0.2	0.1	0.55	0.33
$(NH_4)_2CO_3$	48	0.5	0.03	0.06	0.25	0.5	—	—

a. The final volume of each simulated digestion fluid stock solution was made up to 200 mL with deionized water. Adapted from Minekus et al. (2014).

Gastric phase.
Simulated gastric fluid (SGF) was prepared following the procedure of (Minekus et al., 2014) (Table 2). SGF electrolyte stock solution (6.5 mL, pH 3.0) was mixed with the sample (0.25 g). One mL of porcine pepsin solution (20,000 U/mL) and 0.5 mL of fungal lipase (500 U/mL) were added to the mixture. Fungal lipase was included as an analogue to human gastric lipase (Lecomte et al., 2015). Then, 2.5 μL of 0.3M$CaCl_2$ and 1.99 mL of deionized water were added, and the pH of the final mixture was adjusted to 3.0 with 7.5 μL of 1 M HCl. The mixture was mixed at 37 °C for 2 hr in a shaking water bath at 100 rpm. The pH of the mixture was checked and readjusted to 3.0 with 1 M HCl, if required.

Intestinal phase.
Simulated intestinal fluid (SIF) electrolyte stock solution was prepared according to Minekus et al. (2014; Table 2). SIF electrolyte stock solution (6.125 mL, pH 7.0) was mixed with the sample (0.25 g). Pancreatin solution was made up in SIF electrolyte stock solution based on α-amylase activity. The α-amylase activity of 200 U/mL was achieved in the final mixture by adding 1.25 mL of pancreatin solution (1,600 U/mL). Additional porcine pancreatic lipase (19,655 U) was included into the pancreatin solution to achieve a final lipase activity of 2,000 U/mL. Then, 0.625 mL of fresh bile solution (160 mM, prepared in SIF) and 10 μL of 0.3 M $CaCl_2$ were added to the mixture and the pH was adjusted to 7.0 using 1 M HCl (40 μL). Lastly, 1.95 mL of deionized water was added, and the final mixture was incubated at 37 °C for 2 hr in the shaking water bath at 100 rpm. The pH was monitored throughout the digestion and kept constant at pH 7.0 by adding 1 M HCl.

Sequential oral, gastric and intestinal digestion.
PSNSA-F, PS-NSA-3F, and empty PS-NSA underwent oral, gastric, and intestinal digestions successively to replicate the entire digestion process. First, the sample was exposed to oral digestion as described above and once completed, gastric phase SGF was added and the pH adjusted to 3.0 with 1 M HCl. Afterwards, porcine pepsin, fungal lipase, $CaCl_2$, and deionized water were included as described above. The final ratio of oral bolus to SGF was 50:50 (v/v). This mixture was incubated for 2 hr at 37 °C with agitation at 100 rpm. After the gastric

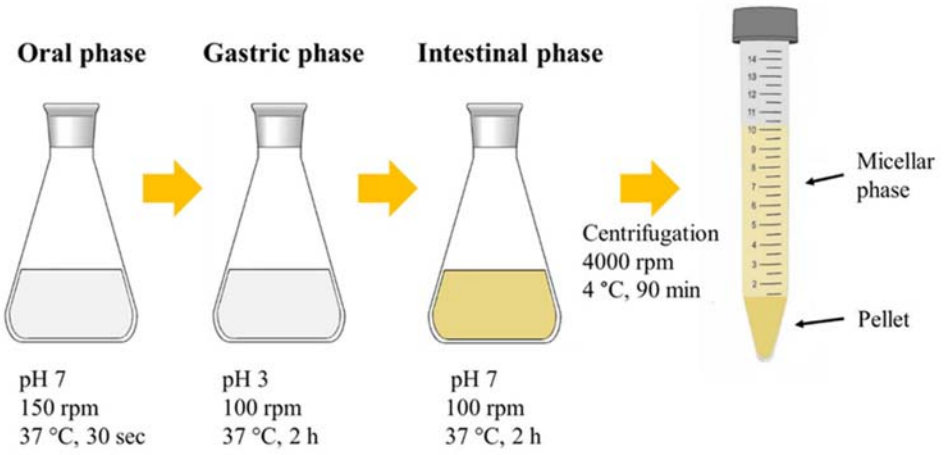

Figure 1. Illustration of the main steps involved in the bioaccessibility determination.

digestion, SIF was added to the mixture and the pH was adjusted to 7.0 with 1 M NaOH. Then, pancreatin, pancreatic lipase, fresh bile, $CaCl_2$, and deionized water were added to the mixture as described in the previous section. The final ratio of the gastric chyme to SIF was 50:50 (v/v). Intestinal digestion lasted 2 hr at 37 °C with agitation at 100 rpm. The pH was readjusted periodically to 7.0 with 1M HCl.

Bioaccessible fraction

The bioaccessible fraction after each of oral, gastric, intestinal and sequential digestions was determined according to the method of Alemany et al. (2013). The workflow involved in the determination of phytosterol bioaccessibility throughout sequential digestion is illustrated in **Figure 1.** Digestion was stopped after each step by immersing the flasks in an ice bath. The bioaccessible fraction (supernatant) of the digested samples was obtained by centrifugation at 4 °C at 4,000 rpm for 90 min using a refrigerated centrifuge (Allegra X-15R, Beckman Coulter, CA, USA). The bioaccessibility (%) of the phytosterols was calculated using the Eq. (1):

$$\textit{Bioaccessibility}\ (\%) = \frac{\textit{Weight of the phytosterols in the bioaccessible fraction}}{\textit{Weight of the total phytosterols included}} * 100 \quad (1)$$

Phytosterol analysis

Phytosterols were quantified by a GC (Hewlett-Packard (HP) 6890 GC, Agilent Technologies, DE, USA) equipped with a flame ionization detector. Briefly, 50 µL of internal standard (5*α*-cholestane, 2.25 mg/mL) was added onto 4 mL of bioaccessible fraction obtained from the simulated digestion. Then, the mixture was subjected to saponification at 40 °C for 1 hr with 4 mL of 1 N KOH in methanol and kept at room temperature (21 °C) for 18 hr. The unsaponifiable fraction was then extracted three times with hexane/methyl *tert*-butyl ether (50:50, v/v). The extract was filtered through 0.45 µm syringe filter (Whatman™, Buckinghamshire, UK) and dried by blowing nitrogen at room temperature. The dry residue was dissolved in 0.3 mL of pyridine and silylated with 1 mL of Sylon BFT at 50 °C for 30 min. The silylated samples were injected onto a GC column (DB-35MS, 25 × 0.20 mm × 0.33 µm; J&W, Agilent Technologies, CA, USA) in the splitless mode with a HP 6890 Series autoinjector. Helium was used as carrier gas at a flow rate of 0.5 L/min. The initial oven temperature was 100 °C for 5 min, then increased to 250 °C at 25 °C/min and hold at 250 °C for 1 min, then increased to 290 °C at 3 °C/min and finally kept at 290 °C for 40 min. The temperatures of the detector and the injector were set to 300 °C and 270 °C, respectively.

Hydrolysis of NSA during in vitro digestion

Reducing sugar concentration in the bioaccessible fraction was determined using 3,5-dinitrosalicylic acid (DNS) method (Miller, 1959). The absorbance measurements were performed with a UV/VIS spectrophotometer (Evolution 201, Thermo Scientific, Waltham, MA, USA) at 540 nm. The number of moles of the reducing sugars was calculated from an external calibration curve with glucose as the standard. The NSA hydrolysis (%) was calculated using the Eq. (2):

$$NSA\ hydrolysis\ (\%) = \frac{Moles\ of\ reducing\ sugars\ in\ the\ bioaccessible\ fraction}{\left(\frac{Weight\ of\ starch}{162}\right)} * 100 \quad (2)$$

Zeta potential measurements

The zeta potential of the bioaccessible fractions obtained after sequential oral, gastric and intestinal digestion was measured using a Zetasizer (Nano ZS, Malvern Instruments Ltd., Worcestershire, UK). The samples were measured at pH 7.0 and 25 °C with 50 continuous readings after an equilibration time of 120 s in triplicate. A blank and empty NSA which were subjected to sequential oral, gastric, and intestinal digestion were also analyzed for their zeta potentials.

Statistical analysis

All experiments performed in triplicate and the data were presented as the mean ± standard deviation. The multiple comparison of the means was carried out by Tukey's test using Minitab® 16.1.1 software (Minitab Inc., State Collage, PA, USA). The differences were considered to be significant when $P < 0.05$.

Results and Discussion

The size of the crude phytosterols ranged between 20 and 150 μm, whereas the size of the phytosterol particles formed (impregnated) in the NSA were 68.0 ± 11.7 and 69.4 ± 9.0 nm for PS-NSA-F and PS-NSA-3F, respectively (**Figure 2**). Both PSNSA-F and PS-NSA-3F generated spherical phytosterol nanoparticles; however, the distribution of the nanoparticles differed with impregnation conditions. PS-NSA-F

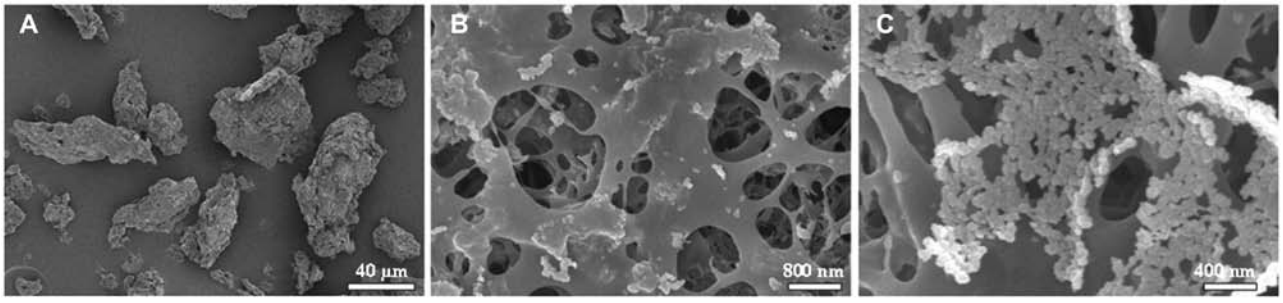

Figure 2. SEM images of (A) crude phytosterols, (B) phytosterol impregnated NSAs at 45 MPa, 90 °C with fast (PS-NSA-F), and (C) three successive fast cooling (PS-NSA-3F).

produced more isolated phytosterol nanoparticles (Figure 2B), whereas PS-NSA-3F generated aggregates of phytosterol nanoparticles (Figure 2C) after three successive depressurizations during impregnation which resulted in higher phytosterol impregnation capacities. The impregnation capacities of NSA-F and PS-NSA-3F were 76.1 ± 1.7 and 101.3 ± 1.8 mg phytosterol/g NSA, respectively. The crystallinity of the phytosterol nanoparticles impregnated into NSA at the same impregnation conditions was investigated by an x-ray diffractometer in our previous study (Ubeyitogullari & Ciftci, 2017). The intensities of the characteristic diffraction peaks of the phytosterol nanoparticles impregnated in the NSAs were much lower than that of crude phytosterols as previously reported, which means reduced crystallinity of phytosterols by impregnation into NSAs (Ubeyitogullari & Ciftci, 2017).

We have previously shown that this novel approach generates low-crystallinity phytosterol nanoparticles (Ubeyitogullari & Ciftci, 2016b). In this method, phytosterols were first dissolved in SC-CO_2 to form a phytosterol-SC-CO_2 solvato complex which diffused into nanopores of the NSAs. Next, phytosterols were precipitated from the phytosterol-SC-CO_2 solvato complex by decreasing the solubility of phytosterols in SC-CO_2 with a sudden decrease in temperature and pressure. NSA prevented the formation of large phytosterol crystals due to a rapid recrystallization. In addition, precipitating phytosterol molecules were not able to organize to form well-ordered phytosterol crystals due to sudden recrystallization. Because of their nanoscale and reduced crystallinity, impregnated phytosterols were 37 times more water soluble than crude phytosterols (Ubeyitogullari & Ciftci, 2016b). Although improved water solubility is an indicator of bioaccessibility, we further assessed bioaccessibility under simulated digestion.

The bioaccessibility of the phytosterols present in the PS-NSA physical mixture, PS-NSA-F and PS-NSA-3F after each phase of digestion (oral, gastric, intestinal, and their sum) is depicted in **Figure 3**. Since the initial phytosterol content of the blank sample and empty NSA were zero, they were not included in Figure 3. As would be expected, there was no phytosterol in the bioaccessible fraction after oral digestion because of the absence of emulsifiers, such as phospholipids, bile salts (Rein et al., 2013), and the short contact time (30 seconds). Similarly, the bioaccessibility of the phytosterols after the gastric phase was very low; 0.6% and 0.4% for PS-NSA-F and PS-NSA-3F, respectively (Figure 3).

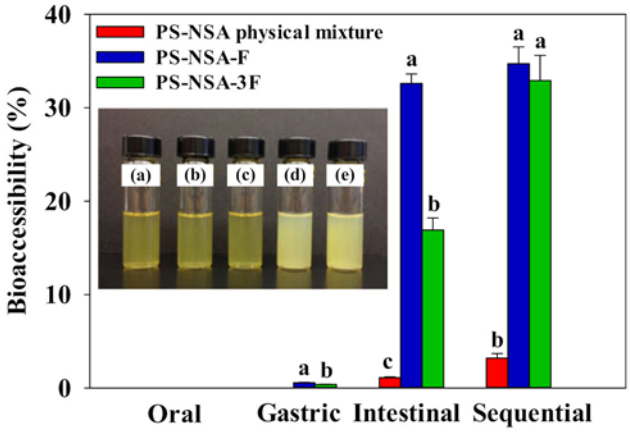

Figure 3. Bioaccessibility of phytosterols after each digestion phase in different samples. Inset image: Gross appearance of the bioaccessible fraction of the (a) blank, (b) empty NSA, (c) physical mixture of crude phytosterols and NSA, (d) phytosterol impregnated NSAs with fast, and (e) successive fast cooling.

Phytosterol bioaccessibility after the intestinal digestion was significantly higher with PS-NSA-F (32.6%) than PS-NSA-3F (16.9%) (Figure 3). The difference was related to the phytosterol aggregates that formed after impregnation and hindered solubility. The aggregates were not stable in the digesta and precipitated during centrifugation. Since the bioaccessibility of PS+NSA physical mixture was low (only 1.1%) after intestinal digestion, the superior bioaccessibility of phytosterols from PS-NSA-F and PS-NSA-3F was mainly due to the low crystallinity and nanosize of impregnated phytosterols. The bioaccessibility of phytosterols was higher after the sequential oral, gastric and intestinal digestion. The bioaccessibility of the phytosterols in the PS-NSA-3F increased from 16.9% to 32.9% when sequential oral, gastric and intestinal digestion was employed rather than just intestinal phase digestion. PS-NSA-F and PS-NSA-3F exhibited similar bioaccessibilities after the sequential oral, gastric, and intestinal digestion: 34.7% and 32.9%, respectively (Figure 3). The bioaccessibilities of phytosterols PS-NSA-F and PS-NSA-3F were much higher than that of phytosterols impregnated into corn starch aerogels (14.3%) in our previous study. However, bioaccessibility of phytosterols (27.7%) was comparable when impregnated into wheat starch aerogels (Ubeyitogullari et al., 2018). Although, the bioaccessibility of phytosterols derived from PS+NSA physical mixture increased ($P < 0.05$), it remained (3.2%) markedly lower than that of PS-NSA-F and PS-NSA-3F.

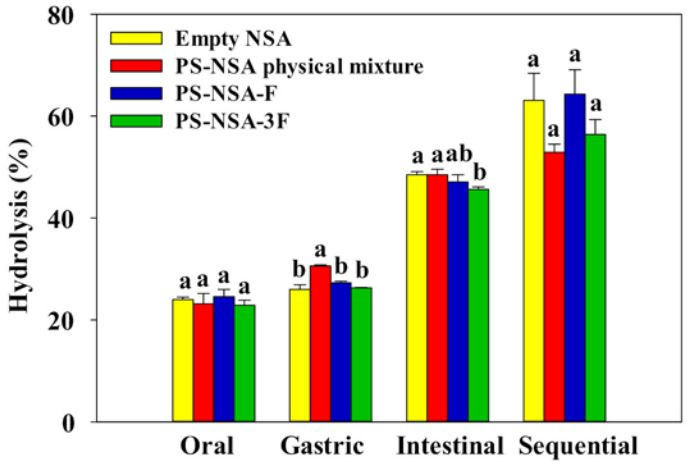

Figure 4. Hydrolysis of the NSA in the samples after each digestion phase.

The gross appearance of the various preparations after sequential oral, gastric and intestinal digestion is shown in Figure 3.We noted the appearance of the blank (vial a), empty NSAs (vial b), and the PS-NSA physical mixture (vial c) was similar and characterized by a clear supernatant; however, the appearance of PS-NSA-F (vial d) and PS-NSA-3F (vial e) was turbid due to the emulsification of phytosterol nanoparticles with bile (Cao, Ou, Lin, & Tang, 2016; Minekus et al., 2014). Since NSA was notably hydrolyzed during oral (25%) and gastric (31%) digestion (**Figure 4**), we infer that phytosterol particles undergoing sequential digestion were more accessible to bile compared to phytosterol particles undergoing intestinal digestion alone. Moreover, phytosterol aggregates underwent disintegration during gastric digestion and formed isolated phytosterol particles which can transfer to the bioaccessible phase during intestinal digestion (Kong & Singh, 2008). It was previously shown that curcumin-loaded lipid nanoparticles which agglomerated during oral digestion were dissociated during gastric digestion due to dilution, pH change, and weakening of particle attraction (Zou et al., 2016). Since PS-NSA-3F lack charged surfactants and charged surfactants results in agglomeration or flocculation of nanoparticles in gastric or intestinal fluids, phytosterol aggregates could be separated and did not agglomerate (Liversidge & Conzentino, 1995).

Although the increase in the bioaccessibility of phytosterols was attributed to the reduced crystallinity, the experimental measurement

of the crystallinity was not possible during and after digestion due to aqueous suspension of the phytosterols in the digestion media. Drying of the digesta prior to XRD analysis results in recrystallization of the phytosterols and therefore crystallinity data attained may not represent the phytosterols in the digesta anymore. Moreover, the other components of the digesta (bile salts and enzymes) interfere with the crystallinity determination. Therefore, it was not possible to determine the effect of digestion on the crystallinity of phytosterol particles in this study. Nevertheless, there is a need for future research and new techniques to determine the crystallinity of phytosterols during the digestion process.

Hydrolysis of NSA was determined after each digestion phase with the DNS method, which quantifies reducing sugars released during digestion of starch (Figure 4). NSA was hydrolyzed (up to 24.6%) by α-amylase during oral digestion. There were no significant differences in the extent of starch hydrolysis among the preparations (empty NSA, PS-NSA physical mixture, PS-NSAF, and PS-NSA-3F) after oral digestion ($P > 0.05$). Hydrolysis of NSA during gastric digestion was approximately 27% and resulted from the chemical breakdown of starch into glucose and oligosaccharides in acidic conditions (Bornhorst & Singh, 2012; Lorenz & Johnson, 1972). Pancreatic α-amylase acted on starch and resulted in approximately 47% hydrolysis during intestinal digestion. Amylase predominantly produces maltose followed by other water-soluble dextrins (for example, maltotriose, maltotetraose, and maltopentaose) from starch (Dona, Pages, Gilbert, & Kuchel, 2010; Tomasik & Horton, 2012). Since the rate of hydrolysis of maltose or maltotriose into glucose is very low, NSA hydrolysis did not increase during sequential oral, gastric, and intestinal digestion, and ranged between 53% and 64% (Figure 4). Moreover, NSA hydrolysis was not affected by the presence of phytosterols, either added in physical mixture or impregnated.

The zeta potentials of the bioaccessible fractions after sequential oral, gastric and intestinal digestion are presented in **Figure 5**. The zeta potential provides information about the stability of the particles by measuring the surface charge (Kesisoglou, Panmai, & Wu, 2007). The zeta potential was highest for the empty NSA (−35.0 ± 0.9 mV) followed by the blank preparation (−29.7 ± 1.0mV). Surface-active anionic species (that is, bile salts) in the intestinal digestion resulted in

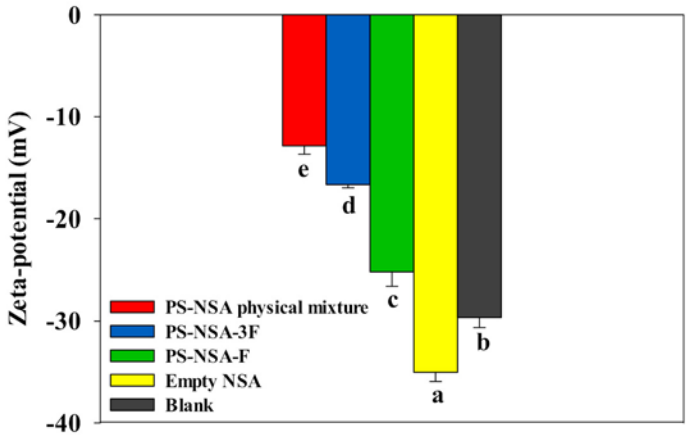

Figure 5. Zeta potential of the bioaccessible fraction of different digested samples.

highly negative zeta potential values (Tangsrianugul, Suphantharika, & McClements, 2015). Likewise, starch digestion products had negative charges due to hydroxyl groups (–OH) (Matsumoto, 1993) and contributed to the increase in the zeta potential of empty NSA. The zeta potentials of PS-NSA-F and PS-NSA-3F were −25.2 ± 1.4 and −16.7 ± 0.3 mV, respectively (Figure 5). As expected, the lowest zeta potential (−12.9 ± 0.8 mV) was obtained with PS-NSA physical mixture. Zeta potential values were in good agreement with our data of phytosterol particle stability in the micellar phase (Figure 3). It is well known that as zeta potential decreases, the electrostatic repulsion between particles decreases which leads to aggregation (Oehlke et al., 2014; Tangsrianugul et al., 2015). Therefore, the relatively low zeta potential of the PS-NSA physical mixture resulted in the precipitation of crude phytosterols during centrifugation.

As previously stated, many techniques including emulsion formation, RESS and DELOS have been used to produce phytosterol particles. However, the majority of these studies did not evaluate the particles under *in vitro* or *in vivo* digestion. Rossi et al. (2010) generated rod-like colloidal phytosterol crystals (particle lengths: 50 to 700 nm and diameters: 80 to 250 nm) by antisolvent precipitation in water from ethanol. In that study, the bioaccessibility of the phytosterols was determined using *in vitro* solubilization with dietary mixed micelles but absence of digestive enzymes. Although 11 wt.% of large phytosterol particles were found in the dietary mixed micellar phase

after 24 hr, the solubilization increased to 40 wt.% with colloidal phytosterols. These values are slightly higher than ours. Possible explanations include (i) the lack of enzymes, (ii) longer reaction times (24 hr), and (iii) the use of filtration prior to quantifying phytosterol concentration. In another study by Cao et al. (2016), protein-based phytosterol nanoparticles (particle size ranging from 123 to 205 nm) were formed by emulsification-evaporation wherein the kinetically stable maximum loading amount was approximately 17 wt.%. *In vitro* bioaccessibility experiments were carried out using sequential gastric (60 min) and intestinal (120 min) digestion. The bioaccessibility of the crude phytosterols and phytosterols encapsulated in protein nanoparticles were 17.8% and 29.2%, respectively. The highest bioaccessibility achieved with impregnated phytosterols in this study (34.7%) was higher than that obtained with protein-based phytosterol nanoparticles (29.2%). However, crude phytosterols had higher bioaccessibility in Cao et al. (2016), an observation possibly due to the phytosterol preparation method (mixing 1 mL of phytosterol-ethanol solution [2% w/v] in 50 mL water) prior to digestion.

In the present study, the bioaccessibility of crude phytosterols was lower than data previously published (Cao et al., 2016; Vaghini, Cilla, Garcia-Llatas, & Lagarda, 2016). One explanation is the absence of other food components (for example, fats) during digestion which contribute to emulsification/micellarization in the intestinal lumen (Alvarez-Sala et al., 2016). Our study clearly shows the superior bioaccessibility of low-crystallinity phytosterol nanoparticles, which stems from gains in water dissolution (owing to the reduction in crystallinity) and micellarization (afforded by particle size reduction). The high phytosterols' bioaccessibility (34.7%) as obtained in this study in the absence of fat suggests broad applications of phytosterol impregnated NSA in nonfat or low-fat food products.

Conclusions

Phytosterol nanoparticles (approximately 69 nm) with reduced crystallinity were successfully generated by impregnation of phytosterols into NSA using SC-CO_2. The bioaccessibility of phytosterols obtained with this approach was significantly improved from 3% to 35%.

Phytosterol nanoparticle aggregates had similar bioaccessibility as isolated phytosterol nanoparticles during sequential oral, gastric and intestinal digestion. The hydrolysis of NSA-containing starch amounted to 64% during sequential digestion and was unaffected by the presence of phytosterols. Zeta potentials of the samples were in a good agreement with bioaccessibility data. This novel, simplified and green approach has the potential to enhance the health benefits of phytosterols by allowing the incorporation of bioavailable phytosterols into nonfat and low-fat functional foods.

Acknowledgments — We gratefully acknowledge the financial support by the United States Department of Agriculture, National Institute of Food and Agriculture (USDA NIFA) (Accession Number 1011129), and the ARD Innovation Fund for Wheat/Cereal Crops and the Wheat/Cereal Scholarship & Fellowship Support Fund (No. 11968).

Author Contributions — A. Ubeyitogullari designed the study, conducted the experiments, collected data, interpreted the results and drafted the manuscript. O. N. Ciftci designed the study, contributed to interpreting the results and drafting the manuscript. R. Moreau and D. J. Rose contributed to interpreting the results.

References

Acevedo, N. C., & Franchetti, D. (2016). Analysis of co-crystallized free phytosterols with triacylglycerols as a functional food ingredient. *Food Research International*, *85*, 104–112. https://doi.org/10.1016/j.foodres.2016.04.012

Aldini, R., Micucci, M., Cevenini, M., Fato, R., Bergamini, C., Nanni, C., . . . Budriesi, R. (2014). Anti-inflammatory effect of phytosterols in experimental murine colitis model: Prevention, induction, remission study. *PLoS One*, *9*(9), e108112. https://doi.org/10.1371/journal.pone.0108112

Alemany, L., Cilla, A., Garcia-Llatas, G., Rodriguez-Estrada, M. T., Cardenia, V., & Alegría, A. (2013). Effect of simulated gastrointestinal digestion on plant sterols and their oxides in enriched beverages. *Food Research International*, *52*(1), 1–7. https://doi.org/10.1016/j.foodres.2013.02.024

Alvarez-Sala, A., Garcia-Llatas, G., Cilla, A., Barberá, R., Sánchez-Siles, L. M., & Lagarda, M. J. (2016). Impact of lipid components and emulsifiers on plant sterols bioaccessibility from milk-based fruit beverages. *Journal of Agricultural and Food Chemistry*, *64*(28), 5686–5691. https://doi.org/10.1021/acs.jafc.6b02028

Amir Shaghaghi, M., Harding, S. V., & Jones, P. J. H. (2014). Water dispersible plant sterol formulation shows improved effect on lipid profile compared to plant

sterol esters. *Journal of Functional Foods*, *6*(Supplement C), 280–289. https://doi.org/10.1016/j.jff.2013.10.017

Bornhorst, G. M., & Singh, R. P. (2012). Bolus Formation and Disintegration during Digestion of Food Carbohydrates. *Comprehensive Reviews in Food Science and Food Safety*, *11*(2), 101–118. https://doi.org/10.1111/j.1541-4337.2011.00172.x

Cao, W.-J., Ou, S.-Y., Lin, W.-F., & Tang, C.-H. (2016). Food protein-based phytosterol nanoparticles: Fabrication and characterization. *Food & Function*, *7*(9), 3973–3980. https://doi.org/10.1039/C6FO00861E

Di Battista, C. A., Constenla, D., Ramírez-Rigo, M. V., & Piña, J. (2015). The use of arabic gum, maltodextrin and surfactants in the microencapsulation of phytosterols by spray drying. *Powder Technology*, *286*, 193–201. https://doi.org/10.1016/j.powtec.2015.08.016

Dona, A. C., Pages, G., Gilbert, R. G., & Kuchel, P. W. (2010). Digestion of starch: In vivo and in vitro kinetic models used to characterise oligosaccharide or glucose release. *Carbohydrate Polymers*, *80*(3), 599–617. https://doi.org/10.1016/j.carbpol.2010.01.002

Feng, S., Dai, Z., Liu, A., Wang, H., Chen, J., Luo, Z., & Yang, C. S. (2017). *β*-Sitosterol and stigmasterol ameliorate dextran sulfate sodium-induced colitis in mice fed a high fat Western-style diet. *Food & Function*, *8*, 4179–4186. https://doi.org/10.1039/ C7FO00375G

Fisher, S., Wachtel, E. J., Aserin, A., & Garti, N. (2013). Solubilization of simvastatin and phytosterols in a dilutable microemulsion system. *Colloids and Surfaces B: Biointerfaces*, *107*, 35–42. https://doi.org/10.1016/j.colsurfb.2013.01.036

He, W.-S., Hu, D., Wang, Y., Chen, X.-Y., Jia, C.-S., Ma, H.-L., & Feng, B. (2016). A novel chemo-enzymatic synthesis of hydrophilic phytosterol derivatives. *Food Chemistry*, *192*, 557– 565. https://doi.org/10.1016/j.foodchem.2015.07.047

Kesisoglou, F., Panmai, S., & Wu, Y. (2007). Nanosizing—Oral formulation development and biopharmaceutical evaluation. *Advanced Drug Delivery Reviews*, *59*(7), 631–644. https://doi.org/10.1016/j.addr.2007.05.003

Kong, F., & Singh, R. P. (2008). Disintegration of solid foods in human stomach. *Journal of Food Science*, *73*(5), R67–R80. https://doi.org/10.1111/j.1750-3841.2008.00766.x

Lecomte, M., Bourlieu, C., Meugnier, E., Penhoat, A., Cheillan, D., Pineau, G., . . . Michalski, M.-C. (2015). Milk polar lipids affect in vitro digestive lipolysis and postprandial lipid metabolism in mice. *The Journal of Nutrition*, *145*(8), 1770–1777. https://doi.org/10.3945/jn.115.212068

Leong, W. F., Lai, O. M., Long, K., Che Man, Y. B., Misran, M., & Tan, C. P. (2011). Preparation and characterisation of water-soluble phytosterol nanodispersions. *Food Chemistry*, *129*(1), 77–83. https://doi.org/10.1016/j.foodchem.2011.04.027

Liversidge, G. G., & Conzentino, P. (1995). Drug particle size reduction for decreasing gastric irritancy and enhancing absorption of naproxen in rats. *International Journal of Pharmaceutics*, *125*(2), 309–313. https://doi.org/10.1016/0378-5173(95)00148-C

Lorenz, K., & Johnson, J. A. (1972). Starch hydrolysis under high temperatures and pressures. *Cereal Chemistry*, *49*, 616–628.

Matsumoto, S. (1993). Proteins and sugars affecting the zeta potential and stability of dispersed vesicular globules in w/o/w emulsions. In K. Nishinari & E. Doi (Eds.), *Food hydrocolloids: structures, properties, and functions* (pp. 399–408). Boston, MA: Springer US.

Meng, X., Pan, Q., & Liu, Y. (2012). Preparation and properties of phytosterols with hydroxypropyl β-cyclodextrin inclusion complexes. [journal article]. *European Food Research and Technology*, *235*(6), 1039–1047. https://doi.org/10.1007/s00217-012-1833-5

Mennah-Govela, Y. A., & Bornhorst, G. M. (2016). Mass transport processes in orange-fleshed sweet potatoes leading to structural changes during in vitro gastric digestion. *Journal of Food Engineering*, *191*, 48–57. https://doi.org/10.1016/j.jfoodeng.2016.07.004

Miller, G. L. (1959). Use of dinitrosalicylic acid reagent for determination of reducing sugar. *Analytical Chemistry*, *31*(3), 426–428. https://doi.org/10.1021/ac60147a030

Minekus, M., Alminger, M., Alvito, P., Ballance, S., Bohn, T., Bourlieu, C., . . . Brodkorb, A. (2014). A standardised static in vitro digestion method suitable for food— An international consensus. *Food & Function*, *5*(6), 1113–1124. https://doi.org/10.1039/C3FO60702J

Moghadasian, M. H., Tan, Z., Le, K., & Shahidi, F. (2016). Anti-atherogenic effects of phytosteryl oleates in apo-E deficient mice. *Journal of Functional Foods*, *21*, 97–103. https://doi.org/10.1016/j.jff.2015.11.031

Moreno-Calvo, E., Temelli, F., Cordoba, A., Masciocchi, N., Veciana, J., & Ventosa, N. (2014). A new microcrystalline phytosterol polymorph generated using CO_2-expanded solvents. *Crystal Growth & Design*, *14*(1), 58–68. https://doi.org/10.1021/cg401068n

Moschakis, T., Dergiade, I., Lazaridou, A., Biliaderis, C. G., & Katsanidis, E. (2017). Modulating the physical state and functionality of phytosterols by emulsification and organogel formation: Application in a model yogurt system. *Journal of Functional Foods*, *33*, 386–395. https://doi.org/10.1016/j.jff.2017.04.007

Nguyen, T. T. (1999). The cholesterol-lowering action of plant stanol esters. *The Journal of Nutrition*, *129*(12), 2109–2112.

Oehlke, K., Adamiuk, M., Behsnilian, D., Graf, V., Mayer-Miebach, E., Walz, E., & Greiner, R. (2014). Potential bioavailability enhancement of bioactive compounds using food-grade engineered nanomaterials: A review of the existing evidence. *Food & Function*, *5*(7), 1341– 1359. https://doi.org/10.1039/C3FO60067J

Othman, R. A., & Moghadasian, M. H. (2011). Beyond cholesterol-lowering effects of plant sterols: Clinical and experimental evidence of anti-inflammatory properties. *Nutrition Reviews*, *69*(7), 371–382. https://doi.org/10.1111/j.1753-4887.2011.00399.x

Ras, R. T., Geleijnse, J. M., & Trautwein, E. A. (2014). LDL-cholesterol-lowering effect of plant sterols and stanols across different dose ranges: A meta-analysis of randomised controlled studies. *The British Journal of Nutrition*, *112*(2), 214–219. https://doi.org/10.1017/S0007114514000750

Rein, M. J., Renouf, M., Cruz-Hernandez, C., Actis-Goretta, L., Thakkar, S. K., & da Silva Pinto, M. (2013). Bioavailability of bioactive food compounds: A challenging journey to bioefficacy. *British Journal of Clinical Pharmacology*, *75*(3), 588–602. https://doi.org/10.1111/j.1365-2125.2012.04425.x

Ribeiro, H. S., Gupta, R., Smith, K.W., vanMalssen, K. F., Popp, A. K., & Velikov, K. P. (2016). Super-cooled and amorphous lipid-based colloidal dispersions for the delivery of phytosterols. *Soft Matter*, *12*(27), 5835–5846. https://doi.org/10.1039/C6SM00601A

Rossi, L., Seijen ten Hoorn, J. W. M., Melnikov, S. M., & Velikov, K. P. (2010). Colloidal phytosterols: Synthesis, characterization and bioaccessibility. *Soft Matter*, *6*(5), 928–928. https://doi.org/10.1039/b911371a

Rozner, S., Aserin, A., Wachtel, E. J., & Garti, N. (2007). Competitive solubilization of cholesterol and phytosterols in nonionic microemulsions. *Journal of Colloid and Interface Science*, *314*(2), 718–726. https://doi.org/10.1016/j.jcis.2007.05.091

Tangsrianugul, N., Suphantharika, M., & McClements, D. J. (2015). Simulated gastrointestinal fate of lipids encapsulated in starch hydrogels: Impact of normal and high amylose corn starch. *Food Research International*, *78*, 79–87. https://doi.org/10.1016/j.foodres.2015.11.004

Tomasik, P., & Horton, D. (2012). Chapter 2—Enzymatic conversions of starch. In H. Derek (Ed.), *Advances in carbohydrate chemistry and biochemistry* (Vol. 68, pp. 59–436). Waltham, MA, USA: Academic Press.

Trautwein, E. A., Duchateau, G. S. M. J. E., Lin, Y., Mel'nikov, S. M., Molhuizen, H. O. F., & Ntanios, F. Y. (2003). Proposed mechanisms of cholesterol-lowering action of plant sterols. *European Journal of Lipid Science and Technology*, *105*(3–4), 171–185. https://doi.org/10.1002/ejlt.200390033

Türk, M., Helfgen, B., Hils, P., Lietzow, R., & Schaber, K. (2002). Micronization of pharmaceutical substances by rapid expansion of supercritical solutions (RESS): Experiments and modeling. *Particle & Particle Systems Characterization*, *19*(5), 327–335. https://doi.org/10.1002/1521-4117(200211)19:5<327::AID-PPSC327>3.0.CO;2-V

Türk, M., & Lietzow, R. (2004). Stabilized nanoparticles of phytosterol by rapid expansion from supercritical solution into aqueous solution. *AAPS PharmSciTech*, *5*(4), e56–e56. https://doi.org/10.1208/pt050456

Türk, M., & Lietzow, R. (2008). Formation and stabilization of submicron particles via rapid expansion processes. *Journal of Supercritical Fluids*, *45*(3), 346–355. https://doi.org/10.1016/j.supflu.2008.01.019

Türk, M., Upper, G., & Hils, P. (2006). Formation of composite drug–polymer particles by co-precipitation during the rapid expansion of supercritical fluids. *The Journal of Supercritical Fluids*, *39*(2), 253–263. https://doi.org/10.1016/j.supflu.2006.04.004

Ubeyitogullari, A., & Ciftci, O. N. (2016a). Formation of nanoporous aerogels from wheat starch. *Carbohydrate Polymers*, *147*, 125–132. https://doi.org/10.1016/j.carbpol.2016.03.086

Ubeyitogullari, A., & Ciftci, O. N. (2016b). Phytosterol nanoparticles with reduced crystallinity generated using nanoporous starch aerogels. *RSC Advances*, *6*(110), 108319–108327. https://doi.org/10.1039/C6RA20675A

Ubeyitogullari, A., & Ciftci, O. N. (2017). Generating phytosterol nanoparticles in nanoporous bioaerogels via supercritical carbon dioxide impregnation: Effect of impregnation conditions. *Journal of Food Engineering*, *207*, 99–107. https://doi.org/10.1016/j.jfoodeng.2017.03.022

Ubeyitogullari, A., Moreau, R., Rose, D. J., Zhang, J., & Ciftci, O. N. (2018). Enhancing the bioaccessibility of phytosterols using nanoporous corn and wheat starch bioaerogels. *European Journal of Lipid Science and Technology*, *121*, 1700229. https://doi.org/10.1002/ejlt.201700229

Vaghini, S., Cilla, A., Garcia-Llatas, G., & Lagarda, M. J. (2016). Bioaccessibility study of plant sterol-enriched fermented milks. *Food & Function*, *7*(1), 110–117. https://doi.org/10.1039/C5FO00458F

Woyengo, T. A., Ramprasath, V. R., & Jones, P. J. H. (2009). Anticancer effects of phytosterols. *European Journal of Clinical Nutrition*, *63*(7), 813–820.

Zou, L., Zheng, B., Zhang, R., Zhang, Z., Liu, W., Liu, C., … McClements, D. J. (2016). Food-grade nanoparticles for encapsulation, protection and delivery of curcumin: Comparison of lipid, protein, and phospholipid nanoparticles under simulated gastrointestinal conditions. *RSC Advances*, *6*(4), 3126–3136. https://doi.org/10.1039/C5RA22834D

Zychowski, L. M., Logan, A., Augustin, M. A., Kelly, A. L., Zabara, A., O'Mahony, J. A., … Auty, M. A. E. (2016). Effect of phytosterols on the crystallization behavior of oil-in-water milk fat emulsions. *Journal of Agricultural and Food Chemistry*, *64*(34), 6546–6554. https://doi.org/10.1021/acs.jafc.6b01722